ELSEVIER

Chemical Engineering Journal 67 (1997) 139–145

Chemical Engineering Journal

Velocity field macro-instabilities in an axially agitated mixing vessel

J.-L. Montes [a,1], H.-C. Boisson [a,2], I. Fořt [b,3], M. Jahoda [c,4]

[a] *I.M.F.T., U.M.R. C.N.R.S./I.N.P.-U.P.S. 5502 Allée du professeur Camille Soula, F-31400 Toulouse, France*

[b] *Faculty of Mechanical Engineering, Czech Technical University Technikâ 4, CZ-16607 Prague 6, Czech Republic*

[c] *Faculty of Chemical Engineering, Prague Institute of Chemical Technology Technickâ 3, CZ-16628 Prague 6, Czech Republic*

Received 27 November 1996; revised 22 April 1997; accepted 24 April 1997

Abstract

The flow pattern produced by a 45° pitched-blade turbine in a fully baffled cylindrical flat-bottomed tank is investigated by a qualitative approach using a laser sheet flow visualisation and a quantitative approach using laser Doppler velocimetry measurements in the turbulent and/or transition regime, with water and glycerine solution as the working liquids. The flow visualisation shows the turbulent macro-instabilities as vortices structures appearing between the turbine and the liquid surface. These macro-structures characterise an organized modification of the flow pattern, creating a transient violent flow activity in the upper part of the vessel which is in contrast with the concept of turbulence as being completely random. The time series and the spectral analysis show a non-stationary, pseudo-periodic phenomenon at a frequency much lower than the blade passage frequency, about 6%, and linearly coupled with the frequency of impeller revolution. This phenomenon is analysed in a volume surrounding the impeller and corresponds to a sharp increase in the intensity of the fluctuating motions when the Reynolds number is increased around 600. Information on the time organization is obtained by a time frequency analysis. We show that the phenomenon is present about 20% of the total time in water and more than 40% in a glycerine solution, for a same impeller rotation speed. © 1997 Elsevier Science S.A.

Keywords: Pitched blade turbine; Macro-instabilities; Laser Doppler velocimetry; Spectral analysis; Wavelet transform

1. Introduction

Mechanically stirred tanks are widely used in industry for a variety of mixing processes [1]. Stirred tanks are used to ease blending, heat transfer, and mass transfer. For several years, most of the studies have been empirical due to the extreme complexity of the flow. In a baffled mixing tank, the flow appears three dimensional, highly turbulent and typically pseudo-periodical due to the rotation of the impeller [2]. In addition, understanding the flow in a stirred vessel and determining the hydrodynamics will improve the prediction of the mixing time and of the power consumption, and also the design of the mixing equipment. For these reasons, several authors have recently described the flow in stirred vessels in different ways: photography, pressure tubes, hot-wire anemometers, laser Doppler velocimetry (LDV) or particle image velocimetry (PIV). Nowadays, in many configurations, complete maps of velocity vectors or turbulence intensity have been either measured or computed: it is possible to say that the mean hydrodynamics is rather well known. Detailed measurements have been performed, especially in the impeller region and the bulk circulation flow, but few above the impeller. The purpose of this study is to analyse the large-scale low-frequency phenomena in a fully baffled cylindrical tank agitated by a 45° pitched-blade turbine (PBT) which creates unsteadiness on the flow pattern and affects the instantaneous angle of discharge of the impeller flow and the whole vessel. A pseudo-periodic phenomenon was first identified by Brůha et al. [3] using a mechanical device, called a "tornado-meter", on the basis of the overall effect of the flow on its environment. This phenomenon has been identified as a macro-instability (MI). In the present study, the local fluctuations, obtained by laser Doppler velocimetry, of the velocity field are measured and interpreted to the light of flow visualisations.

[1] Tel: +33 5 61 28 58 33; fax: +33 5 61 28 58 85; e-mail: montes@imft.fr

[2] Tel: +33 5 61 28 58 33; fax: +33 5 61 28 58 99; e-mail: boisson@imft.fr

[3] Tel: +420 2 332 27 13; fax: +420 2 243 10 292.

[4] Tel: +420 2 2435 3233; fax: +420 2 311 73 35; e-mail: jahodam@vscht.cz

PII S1385-8947(97)00042-9

2. Turbulent macro-instability

Variations in flow pattern and discharge angle have been examined in the past. For a marine propeller, Winardi and Nagase [4] report that the flow in the mixing vessel fluctuates in a space scale of the order of the vessel size and in a large time scale. A similar phenomenon has been reported by Nouri and Withelaw [2] and by Kresta and Wood [5], where the circulation pattern is unstable and a secondary circulation loop, in the lower corner of the tank, appears with the primary circulation loop. For them, this phenomenon depends on the Reynolds number and on the off-bottom clearance of the impeller. Chapple and Kresta [6], from visual observations, link the stability of the flow with the geometrical configuration and the turbulent intensity. For Bakker and Van den Akker [7,8], with an axial flow impeller, two opposite vortices motions interact. The interaction between these vortices may lead to instabilities in the flow. Brůha et al. [3] characterise the turbulent flow macro-instabilities by the existence of eddies whose size and, especially, time scales considerably exceed those of current turbulent eddies. From visual observations, the turbulent macro-instabilities are demonstrated to be linked to the macro-eddies in the area between the impeller and the free surface of the liquid. These vortices structures are able to alter the surface if they are sufficiently energetic. In this case, the single-loop flow pattern switches to the double-loop one.

The phenomenon appears in the low frequency range. It is non-stationary, pseudo-periodic and linearly coupled with the blade passage frequency (f_{BP}).

3. Experimental set-up and data processing

The experiments were carried-out in a cylindrical glass vessel of diameter $T=300$ mm with a flat bottom and four baffles of width $W=0.1T$, equally spaced at the tank wall. The tank was filled with the working fluid to a height equal to the diameter ($H=T$). It was surrounded by an outer square glass tank, filled with the same working fluid, in order to minimise the effects of vessel curvature on the intersecting beams and thus on the optical distortion. The impeller was a pitched-blade turbine (PBT) of diameter $D=0.333T$ with six equi-spaced blades inclined at 45°. The blade width was $h=0.2D$. The off-bottom impeller clearance was $H_2=0.35T$ (see Fig. 1). The PBT pumped the liquid towards the vessel bottom. For this study, the geometrical parameters were kept constant. The working liquids were distilled water and two

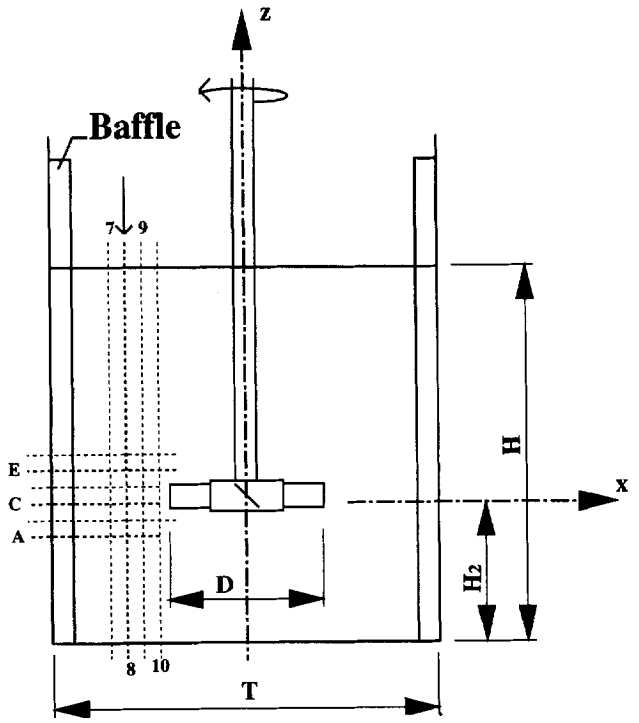

Fig. 1. Vessel details and dimensions.

aqueous glycerine solutions. The physical properties of liquids and the range of impeller speeds are presented in Table 1.

The measurements were performed with a laser 5 W Argon-Ion. The single component LDV works in dual-beam mode with a Bragg cell. The intersection of two laser beams of wavelength $\lambda=514.5$ nm formed the measuring volume, which had a diameter of 0.278 mm, a length of 6.672 mm and fringe spacing of 6.1793 μm. The Doppler signal is analysed using the PDA processor, based on the covariance principle. The radial and/or axial component of liquid velocity are measured at various points in the system. The vessel was horizontally and vertically divided into a network of experimental points as shown in Fig. 1. The horizontal lines are referenced by capital letters A, C ($z=0$) and E, and the vertical lines by Figs. 7–10. For each experimental point and two components of velocity (axial and radial), the recording time of the instantaneous signals was about 25 min. In order to obtain a nearly continuous Doppler signal, the data rate (number of tracer particles per second) was set to about 330 Hz. Thus, 500 000 experimental samples were recorded. The measurements were made in the turbulent and/or transition regime for mixing Reynolds numbers presented in Table 1 and defined by the relation (in SI units)

Table 1
Experimental conditions (at 23 °C)

Liquid	Density ρ/kg m^{-3}	Viscosity μ/Pa s	Impeller speed N/rpm	Re
Water	1000	0.001	450–600	75000 – 1E+05
Glycerin 85%	1221	0.106	200–700	380–1340
Glycerin 91%	1236	0.155	200–700	300–950

$$Re = \frac{\rho N d^2}{\mu} \quad (1)$$

The signal looks random so that it is difficult to extract any information from the time series. The exploitation of the laser signal has been effective with the use of different tools in signal processing, particularly with the fast Fourier transform and the wavelet transform. The spectral analysis via a fast Fourier transform is a way to examine the overall characteristics of the signal. The final power spectrum is an average of 15 power spectra obtained by Fourier transforming of the autocorrelation function of the velocity signal with 32 768 points. The wavelet transform is a compromise between the time evolution and the spectral distribution [9,10]. This transform is obtained by the convolution of the signal with a variable size waveform which is the wavelet. The wavelet is stretched and shrunk continuously along the time axis and systematically compared with the signal at each frequency. The result of this convolution is a quantitative measure of the adaptation of the width and the position of the wavelet. It is introduced by means of a translation fixed by the coefficient α and a dilatation fixed by the coefficient β. The wavelet transform $F(\alpha,\beta)$ is defined in general as

$$F(\alpha,\beta) = \sqrt{\alpha}\int_R \hat{S}(k)\,\hat{\Phi}(\alpha k)\,e^{ik\beta}\mathrm{d}k \quad (2)$$

where $\hat{S}(k)$ is the Fourier transform of the initial signal $S(t)$ and $\hat{\Phi}(k)$ the Fourier transform of the wavelet $\Phi(t)$. We use a Morlet wavelet, complex and localized with a Gaussian envelope, defined as

$$\Phi(t) = e^{ik_0 t}\,e^{-t^2/2} \quad (3)$$

$$\hat{\Phi}(k) = e^{-1/2(k-k_0)^2} \quad (4)$$

The wavelet transform is a band-pass filter centred on the frequency k_0. It enables the different influences to be separated and their evolution in a time-frequency domain to be followed [11].

4. Results and discussion

4.1. High Reynolds number phenomenon

Fig. 2 shows a time series of the axial velocity signal in water for the point E10 (see Fig. 1). The flow is turbulent and $Re = 75\,000$. The signal looks chaotic, but the power spectrum (see Fig. 3) reveals two dominant frequencies. One is the blade passage frequency, corresponding to the frequency of revolution of the impeller ($f_{BP} = N.n_b$). It is observed when the measurement point is close to the impeller and these fluctuations drop rapidly in the bulk of the tank. Such a behaviour has been found by many authors, including Costes and Couderc [12], and is sometimes called a "pseudoturbulent" phenomenon. The second is much lower than the f_{BP} (about 1.5% of the BPF) and is linked with the impeller frequency N by the relation $f_{MI} = 0.0575N$. Montes et al. [13] have analysed this part in more detail.

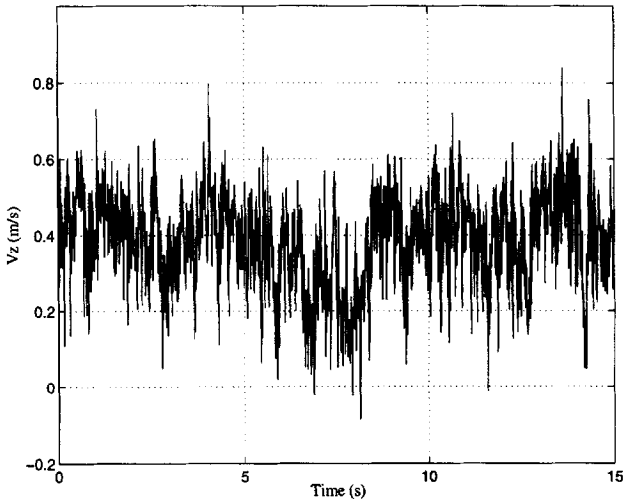

Fig. 2. Time series of the instantaneous axial velocity for the point E10 (water, $N = 450$ rpm).

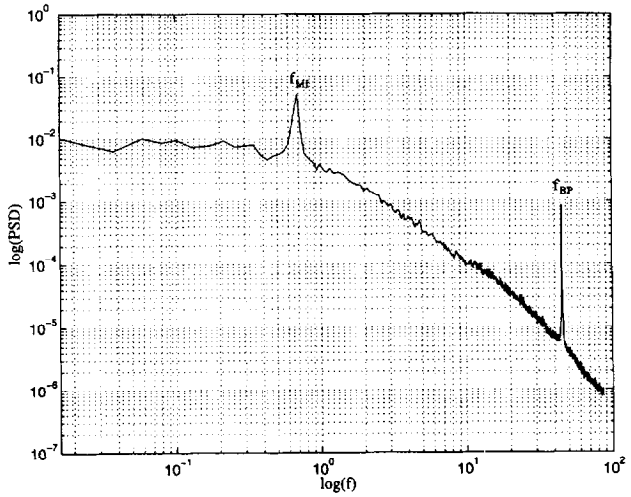

Fig. 3. Frequency spectrum for the axial velocity for the point E10 (water, $N = 450$ rpm).

In water, it is very difficult to identify the macro-instability by visualisation. Even if the shaft run-out is negligible and no special motion appears at the free surface, the low-frequency fluctuation is observed. Moreover, the blade passage and/or the trailing vortices associated with the rotation of the impeller are found in a significantly higher frequency range. Thus, we have worked with a low Re, in a glycerine solution, but with the same impeller speed, 450 rpm. With the help of the visualisation, it is possible to observe the low frequency motion associated with the vortex passage frequency (f_{MI}).

4.2. Transition phenomenon

4.2.1. Visual observation

In the present work, the occurrence of the macro-instability is observed using a laser sheet flow visualisation. The typical vortex pattern is shown in a vertical section between two

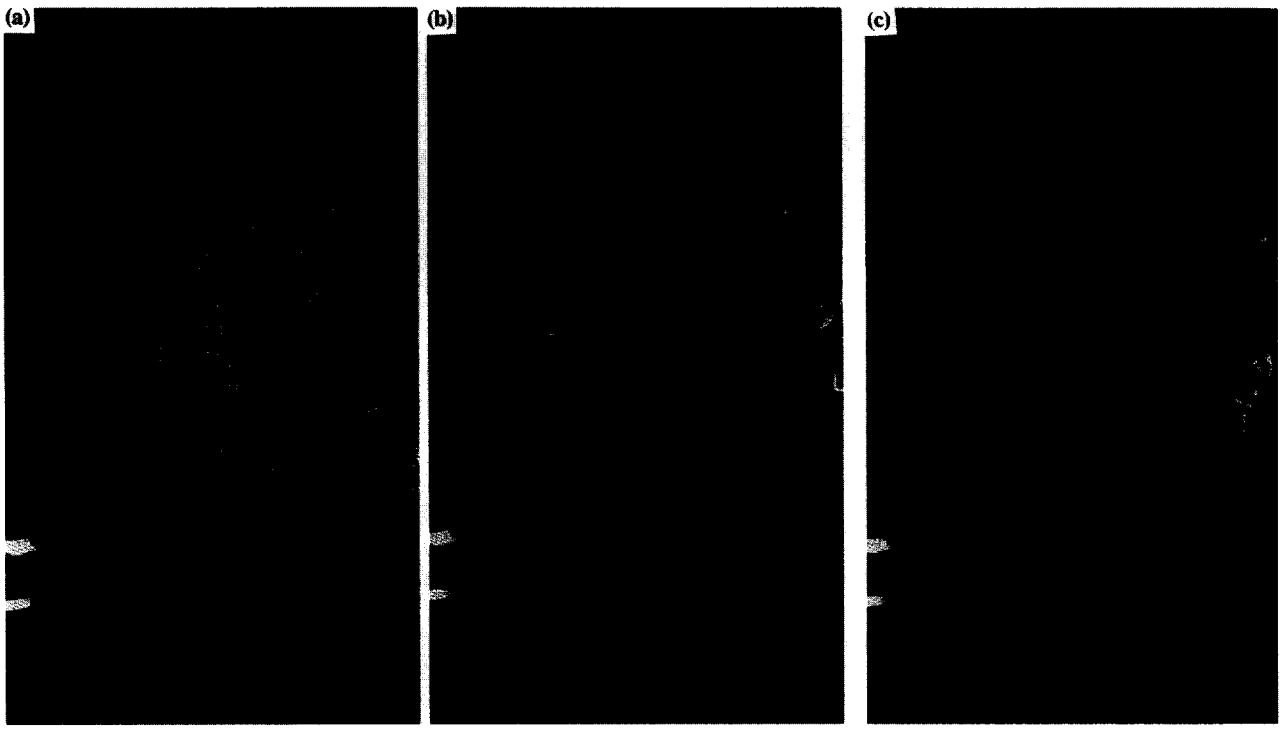

Fig. 4. Illustration of phenomenon evolution in the glycerine, for $Re = 1140$.

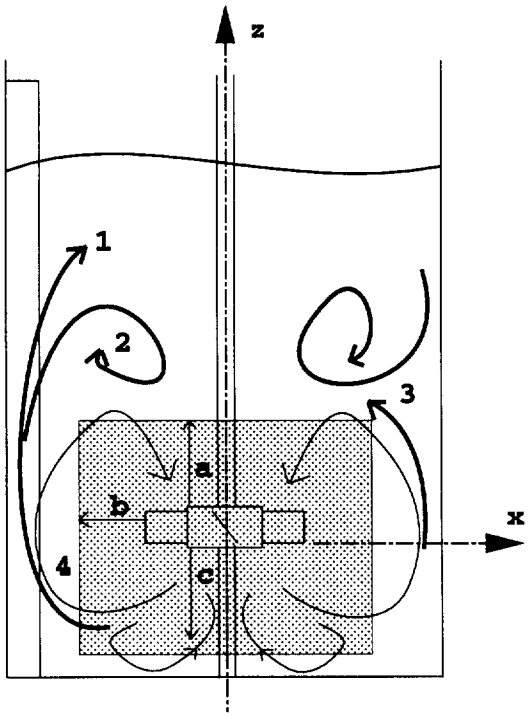

Fig. 5. Representation of the influence area of the MI in the vessel (shaded area) and illustration of different flow patterns: (1) (2) in front of the baffles, (3) between the baffles, (4) in the mean flow.

adjacent baffles (see Fig. 4). The main toroidal loop is visible around the impeller and the formation of a secondary loop can be observed above the impeller. The occurrence of the macro-instability is accompanied by the presence of this upper vortex. The flow in the vessel is three-dimensional. We distinguish two main kinds of flow patterns, one in front of the baffles and the other between the baffles.

The flow pattern is also a function of impeller speed. At lower impeller speeds, it is symmetrical and corresponds to the description by Oldshue [1]: in the whole vessel, the flow pattern appears as a toroidal structure corresponding to a single loop in the water or two loops in the glycerine solutions (this motion corresponds to pattern number 4 in Fig. 5). When the impeller speed increases, the flow pattern becomes asymmetrical. The loops, formerly stable, become unstable with fluctuating dimensions. The centre of the main loop can be shifted in the vertical direction by four or five centimetres. Then the flow macro-instability appears.

The impeller generates streams that reach the bottom, turn, and rise along the vessel wall towards the liquid surface. For the volume of fluid located in front of a baffle and rising along it, we found a part that turns around the baffle and returns into the impeller region. But when the flow speeds up along the baffle and reaches the liquid surface, it creates a deformation of the liquid surface. If this flow is not energetic enough, a strong vertical vortex appears in front of the baffle without reaching the free surface. These motions are sketched in Fig. 5 and correspond to patterns numbers 1 and 2.

When we observe the flow between the baffles, the main vortex sometimes becomes unstable, fluctuating back and forth, pumping like a "heart". From time to time a violent acceleration of the flow occurs from the main vortex towards the liquid surface. The stream from the baffle area flowing down along the wall collides with the rising ejection and both are deviated inside the tank. A vertical vortex is formed (pattern number 3 in Fig. 5). If we use a glycerine solution, the

second loop visible in the lower corner of the tank disappears when a macro-instability is formed. The fluctuations of the main vortex cause some variations in the angle of the impeller discharge flow, which have been analysed by Brůha et al. [14].

In all cases, these vortices appear between the impeller and the liquid surface and can alter this surface in their disintegration phase. In spite of an apparent random character, when the different flow patterns take place, an organized, non-stationary and pseudo-periodic phenomenon is observed. Similarly, Haam et al. [15] observed a low frequency period associated with an axial vortex rotating around the shaft, further disappearing, repeated again and again. The connection between the changes in the flow pattern and the low-frequency oscillations in the vessel has been demonstrated by Brůha et al. [14] using a mechanical device. Owing to the fact that the low frequency observed in the velocity signal is close to the one found by these authors, this frequency can be taken as the signature of the previously described vortex motion.

4.2.2. *Evolution of the spectra*

The evolution of the phenomenon as a function of the Reynolds number is described in this section. From the spatial evolution of the spectra we find that the f_{MI} appears in an area near the impeller. It corresponds to a cylindrical zone whose dimensions are sketched in Fig. 5 (a, b and c), in which the axial and radial velocities and the power spectra are determined for various values of the viscosity and the impeller speed. The spatial evolution of the spectra (PSD ($m^2\ s^{-2}\ Hz^{-1}$) versus frequency (Hz) and position (mm)) is presented in Figs. 7–10 in a glycerine solution (85%) along the vertical level 8 (shown in Fig. 1 with an arrow) below and above the impeller and for two impeller speeds: 200 rpm and 600 rpm (respectively $Re = 380$ and $Re = 1140$).

For $Re = 380$, there is a difference between the spectra above and below the impeller. Fig. 7 shows the influence of the blade passage which is very important in the zone below

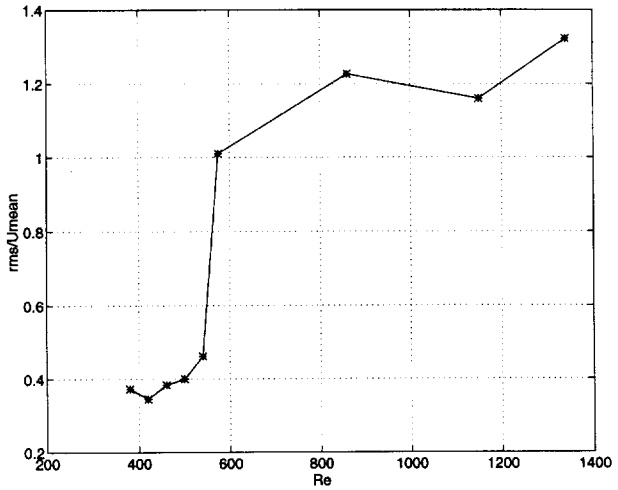

Fig. 6. Variation of velocity fluctuation as a function of Reynolds number (point C8).

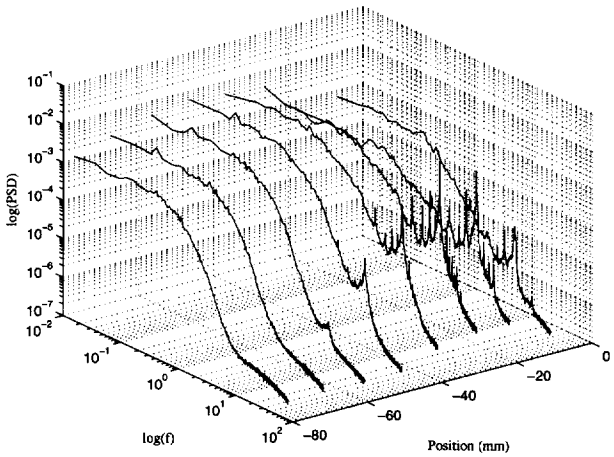

Fig. 7. Spectra below the impeller for impeller speed 200 rpm ($Re = 380$). $z \epsilon [-80\ mm; -10\ mm]$.

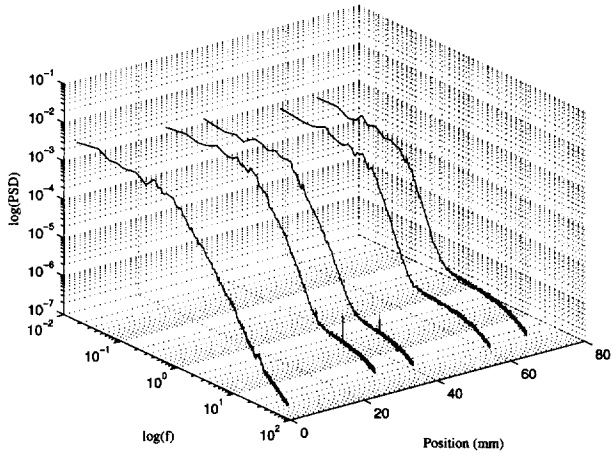

Fig. 8. Spectra above the impeller for impeller speed 200 rpm ($Re = 380$). $z \epsilon [0\ mm; 70\ mm]$.

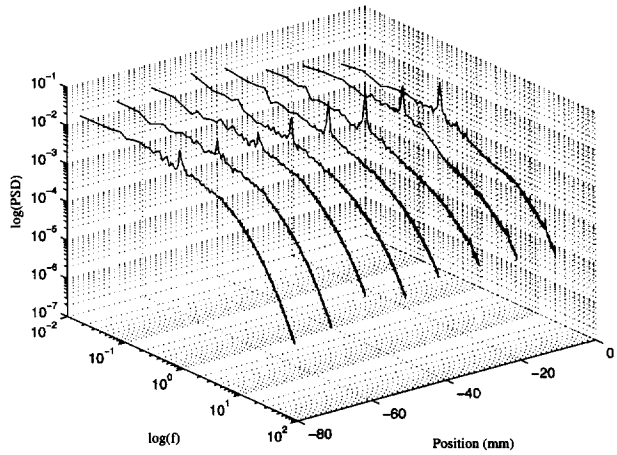

Fig. 9. Spectra below the impeller for impeller speed 600 rpm ($Re = 1140$). $z \epsilon [-80\ mm; -10\ mm]$.

the impeller and practically non-existent above it (see Fig. 8). Below the impeller, centred on the f_{BP} (20 Hz), many harmonics appear as a combination of the number of blades. We are in the impeller discharge stream region. The f_{MI} is not present but we can observe a broad-band low-frequency spectrum. This suggests that random low-frequency motion exists

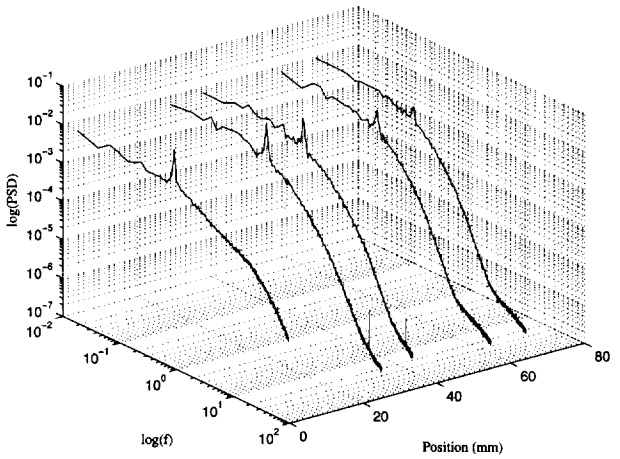

Fig. 10. Spectra above the impeller for impeller speed 600 rpm ($Re = 1140$). $z \in [0\ \text{mm}; 70\ \text{mm}]$.

at this Reynolds number. When we observe the spectra for $Re = 1140$, they look different from the previous ones. Below the impeller (see Fig. 9), there is no visible trace of the f_{BP}. But we can clearly identify the f_{MI} (0.9 Hz) in this region and also above the impeller (see Fig. 10). It is useful to plot the ratio of root mean square velocity fluctuations versus average velocity. Fig. 6 shows a sudden rise in the fluctuations intensity that occurs at a Reynolds number around 600. This result is in good agreement with Brûha et al. [14] who show that a bifurcation in the impeller discharge angle occurs when the Reynolds number reaches 650. The angle can fluctuate between a minimum and maximum value, limits of the instability of the main vortex. From the spectra, it can be observed that not only the pseudo-periodic phenomenon seems to bring energy to the fluctuations but also the whole spectrum is increased. This implies that the production of turbulence is also enhanced.

4.2.3. *Time-frequency analysis*

The time study of the instantaneous power spectrum was realised using the wavelet transform also referred here as time-frequency analysis. The maps of the power spectral density (PSD) versus frequency and time are represented on Fig. 11 for water and Fig. 12 for the 85% glycerine–water solution at the same impeller speed and at a fixed point E7 (see Fig. 1). The peaks, for the power, correspond to white areas in these figures. They are localized in the neighbourhood of the f_{MI}.

From these figures it can be seen that these peaks are observed intermittently and that the phenomenon is clearly more regular in the case of the glycerine solution which is at a lower Reynolds number. A quantitative study can be made on the complete duration of the signal, comparing the PSD to a prescribed threshold value. The intermittent factor (ratio of the time where the PSD is greater than the threshold to the total time) is evaluated to 20% at higher Reynolds number and to more than 40% at the lower one. This method provides a quantitative approach to the regularity of the periodic phenomenon which appears to become more random when the Reynolds number increases. This justifies the interest in studying lower Reynolds numbers in order to give a better description of the behaviour of the flow macro-instability.

5. Conclusions

By means of LDV measurements and flow visualisation, the hydrodynamic properties of the PBT in the baffled mixing

Fig. 11. Wavelet transform in water ($Re = 75\,000$).

Fig. 12. Wavelet transform in a glycerine solution ($Re = 860$).

vessel have been investigated. The experimental study reveals a low-frequency non-stationary pseudo-periodic phenomenon identified as a macro-instability (MI).

The macro-instability which appears as the switching between one loop and two or many loops, takes place between the impeller and the free surface and is able to alter this surface. Different flow patterns are found, in front of the baffles or between two adjacent baffles. The mechanism is complex and three-dimensional but the large vortices clearly appear in a regular way.

It has been found that the f_{MI} is much lower than the f_{BP} (around 1.5%) and linearly coupled with the impeller frequency. Above $Re = 600$, the main vortex becomes unstable, the fluctuations flow increases rapidly, and the angle of impeller discharge fluctuates. The flow induced by a PBT is then more complex than one single loop: with the macro-instability, different flow patterns appear, creating vortices structures in the upper part of the vessel.

With the time-frequency analysis, we have observed the regularity of appearance of this pseudo-periodic component as a function of the liquid viscosity and thus as a function of the Reynolds number for the same impeller speed. Highly periodic events appear regularly for lower Reynolds numbers and in a more random way in higher Reynolds numbers. The presence of this frequency is without doubt linked to the global effects observed by Brůha et al. [14] and is considered as a basic mechanism for the large scale motions in the agitated liquid, taking into account their effects on mixing and on dynamic effects on solid surfaces inside the vessel.

6. Nomenclature

D	diameter of the impeller/mm
f_{MI}	frequency of macro-instability/Hz
f_{BP}	blade passage frequency/Hz
h	width of the blade/mm
H	height of the liquid in the tank/mm
H_2	impeller clearance from the tank bottom/mm
n_b	number of impeller blades
N	impeller speed/min^{-1}
Re	Reynolds number (dimensionless)
T	diameter of the tank/mm
W	width of the baffles/mm
x	radial co-ordinate/mm
z	axial co-ordinate/mm

Greek symbols

ρ	density of liquid/kg m^{-3}
μ	viscosity of liquid/Pa s

Acknowledgements

This work has received the financial support of the European Community under Contract Number CIPA-CT-93-0147 in the form of a Joint Research Project between France and Czech Republic. The authors wish to thank Dr J. Bertrand and Dr C. Baudou for their scientific collaboration, Dr D. Faghani for helping in the data analysis and Mr J.C. Henge and A. Miré for their technical contribution to the experiments. They also thank Dr O. Brůha, Mr P. Smolka, Prof. M. Severa and Dr Z. Chara for their participation in the JRP.

References

[1] J.Y. Oldshue, Fluid Mixing Technology, Chemical Engineering, McGraw-Hill Publications Co., New York, 1983.
[2] J.M. Nouri, J.H. Withelaw, Flow characteristics of stirred reactors with newtonian and non-newtonian fluids, AIChE J. 36(4) (1990) 627–629.
[3] O. Brůha, I. Fořt, P. Smolka, Large scale unsteady phenomenon in a mixing vessel, in: Proc. of Workshop'93, CTU Prague, pp. 59–60.
[4] S. Winardi, Y. Nagase, Unstable phenomenon of flow in a mixing vessel with a marine propeller, J. Chem. Eng. Jpn. 24(2) (1991) 243–249.
[5] S.M. Kresta, P.E. Wood, The mean flow filed produced by a 45° pitched blade turbine: changes in the circulation pattern due to off-bottom clearance, Can. J. Chem. Eng. 71 (1993) 42–53.
[6] D. Chapple, S. Kresta, The effect of geometry on the stability of flow patterns in stirred tank, Chem. Eng. Sci. 49(21) (1994) 3651–3660.
[7] A. Bakker, H.E.A. Van den Akker, Gas-liquid contacting with axial flow impellers, Trans. IChemE 72(Part A) (1994) 573–582.
[8] A. Bakker, H.E.A. Van den Akker, Single-phase flow in stirred reactors, Trans. IChemE 72(A) (1994) 583–593.
[9] J. Liandrat, F. Moret-Bailly, The wavelet transform: some applications to fluid dynamics and turbulence, Eur. J. Mech., B/Fluids, 9(1) (1990) 1–19.
[10] M. Farge, Wavelet transforms and their applications to turbulence, Annu. Rev. Fluid Mech. 24 (1992) 395–457.
[11] J. Martinez, Méthodes temps-fréquence appliquées à l'analyse de signaux d'écoulements turbulents, Thèse de PhD, ENSAE, Toulouse, France, 1994.
[12] J. Costes, J.P. Couderc, Study by laser Doppler anemometry of the turbulent flow induced by a Rushton turbine in a stirred tank: influence of the size of the units-II. Spectral analysis and scales of turbulence, Chem. Eng. Sci. 43(10) (1988) 2765–2772.
[13] J.L. Montes, H.C. Boisson, I. Fořt, Z. Chara, Analyse du comportement non-stationnaire des instabilités de basse fréquence d'un système agité axialement, in: 12e Congrès Français de Mécanique, Vol. 3, pp. 285–289.
[14] O. Brůha, I. Fořt, P. Smolka, M. Jahoda, Experimental study of turbulent macroinstabilities in an agitated system with axial high-speed impeller and with radial baffles, Collect. Czech. Chem. Commun. 61 (1996) 856–867.
[15] S. Haam, R.S. Brodkey, J.B. Fasano, Local heat transfer in a mixing vessel using heat flux sensors, Ind. Eng. Chem. Res. 31(5) (1992) 1384–1391.